Journal of Environmental Radioactivity 295 (2026) 107962

Contents lists available at ScienceDirect

Journal of Environmental Radioactivity

journal homepage: www.elsevier.com/locate/jenvrad

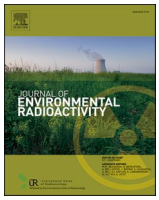

A comparative study of ^{7}Be in total suspended particles (TSP) and PM_{10}

E. Gordo [a,*], E. Liger [b], E.M. Navarro [a], J. Rodríguez-Jiménez [b,c]

[a] Servicios Centrales de Apoyo a la Investigación, Universidad de Málaga, Málaga, Spain
[b] Departamento de Física Aplicada II, Universidad de Málaga, Málaga, Spain
[c] Centro Oceanográfico de Málaga (COMA-IEO), CSIC, Explanada de San Andrés (muelle 9), Puerto de Málaga, Málaga, Spain

ARTICLE INFO

Keywords:
^{7}Be
Aerosol particles
Atmospheric radioactivity
Gamma spectrometry

ABSTRACT

This study evaluates potential differences in ^{7}Be activity concentrations measured using two aerosol sampling systems equipped with PM_{10} and total suspended particles (TSP) inlets under real atmospheric conditions. During the study period, mean ^{7}Be activity concentrations were 4.4 ± 1.4 mBq m^{-3} for PM_{10} and 3.7 ± 1.2 mBq m^{-3} for TSP samples. A strong temporal correlation was observed between both datasets ($\rho = 0.882$, $p < 0.001$), indicating consistent response to atmospheric variability. Although individual weekly differences are not always statistically significant when measurement uncertainties are considered, the overall distribution revealed a systematic tendency toward higher ^{7}Be concentrations in the PM_{10} fraction, with relative differences ranging from 4% to 44%, consistent with the preferential association of ^{7}Be with fine aerosol particles.

Six sampling weeks showed higher ^{7}Be values in TSP than in PM_{10}, but only three met the criterion for statistically significant difference. Back-trajectory analysis showed that only one sampling week corresponded to a well-defined Saharan dust intrusion, whereas the two other cases were more linked to regional resuspension processes and accumulation of locally or regionally derived coarse particles that may enhance the relative contribution of the TSP fraction. These findings indicate that episodic increases of ^{7}Be in the TSP fraction may arise from both mineral dust advection and locally driven coarse-particle accumulation.

Multivariate analysis identified two dominant atmospheric regimes controlling radionuclide variability. The first component linked ^{7}Be concentrations with temperature and wind direction, reflecting the influence of large-scale atmospheric transport and vertical mixing processes. The second component grouped dust concentrations and wind speed, indicating the importance of mechanically driven aerosol resuspension and transport. Overall, the results demonstrate that while PM_{10} and TSP sampling systems provide highly comparable measurements of atmospheric ^{7}Be activity, differences in particle size distribution during dust transport episodes can lead to systematic variations between both fractions. These findings highlight the importance of considering inlet-dependent size selectivity when comparing long-term radionuclide records obtained using different aerosol sampling configurations.

1. Introduction

Beryllium-7 (^{7}Be) is a cosmogenic radionuclide produced in the upper troposphere and lower stratosphere by spallation reactions of cosmic rays with atmospheric nitrogen and oxygen nuclei (Lal and Peters, 1967). The variability in activity of ^{7}Be in surface air is the product of interaction of three processes: production, transport, and deposition. Once formed, ^{7}Be rapidly attaches to atmospheric aerosols and is transported downward to the Earth's surface through large-scale atmospheric circulation and deposition processes (Feely et al., 1989; Baskaran, 2011). Measurements of surface ^{7}Be radioactivity are useful for studying short-term atmospheric transport processes. Temporal variations in the surface ^{7}Be radioactivity were reported at many sites in the world and transport processes of air mass were discussed. Due to its relatively short half-life (53.3 days) and strong affinity for particulate matter, ^{7}Be has been widely used as a tracer of atmospheric transport, aerosol dynamics, and stratosphere–troposphere exchange (e.g., Koch et al., 1996; Dibb et al., 2003; Dueñas et al., 2011).

The measurement of ^{7}Be in surface air is commonly performed by collecting airborne particles on filters using different sampling systems.

This article is part of a special issue entitled: ENVIRA2025 published in Journal of Environmental Radioactivity.

* Corresponding author.
E-mail address: elisagp@uma.es (E. Gordo).

https://doi.org/10.1016/j.jenvrad.2026.107962
Received 18 January 2026; Received in revised form 13 March 2026; Accepted 15 March 2026
Available online 17 March 2026

Among these, PM_{10} samplers, which selectively collect particles with aerodynamic diameters smaller than 10 μm, are frequently employed in air quality monitoring networks, while Total Suspended Particle (TSP) samplers collect a broader size range of aerosols (UNSCEAR, 2000). Since ^{7}Be is predominantly associated with fine and accumulation-mode particles, its measured activity may depend on the sampling methodology and particle size fraction considered (Papastefanou, 2006; Ioannidou and Paatero, 2014). However, direct comparisons between PM_{10} and TSP sampling systems remain limited, and the extent to which sampling configuration influences ^{7}Be quantification is still not fully understood.

Meteorological conditions play a crucial role in controlling the atmospheric concentration and variability of ^{7}Be. Parameters such as temperature, precipitation, wind speed, and wind direction influence aerosol transport, vertical mixing, and removal processes, thereby affecting surface-level ^{7}Be activities (e.g., Błażej and Mietelski, 2014; Gordo et al., 2015; Ioannidou and Papastefanou, 2020). In particular, strong winds and dust resuspension events may alter the relative contribution of coarse and fine particles, potentially modifying the apparent distribution of ^{7}Be between different particulate fractions.

In this context, the present study aims to compare ^{7}Be concentrations measured using PM_{10} and TSP sampling systems and to assess the influence of meteorological variables on the observed differences. Multivariate statistical techniques, such as VARIMAX-rotated Factor Analysis, are applied to identify the main processes governing ^{7}Be behavior and dust dynamics. This approach provides insight into the combined effects of atmospheric transport, meteorology, and sampling methodology on ^{7}Be measurements, contributing to a better interpretation of long-term radionuclide monitoring data.

2. Material and methods

2.1. Sampling site and aerosol collection

An airborne aerosol sampling campaign was carried out at the University of Málaga (36°42′56″ N, 4°28′25″ W), located in southern Spain (Fig. 1). The site is situated about 5 km inland from the Mediterranean coastline and can be classified as an urban background station influenced by both continental and marine air masses. The station forms part of the Environmental Radioactivity Monitoring Network operated by the Spanish Nuclear Security Council (CSN), ensuring standardized procedures, routine quality control, and national-level data comparability.

Airborne dust samples were periodically collected from February 2024 to January 2025 using two high-volume aerosol sampling systems operating in parallel (Fig. 2). Sampling and sample preparation were carried out following the environmental radiological surveillance procedures established by the Consejo de Seguridad Nuclear (CSN, 2005; updated in 2025). Each sampler operated continuously over one-week intervals, with aerosol particles collected on a single filter during each sampling period. Thus, every filter represents an integrated weekly sample, providing average ^{7}Be activity concentrations and reducing the influence of short-term atmospheric variability. Throughout the study

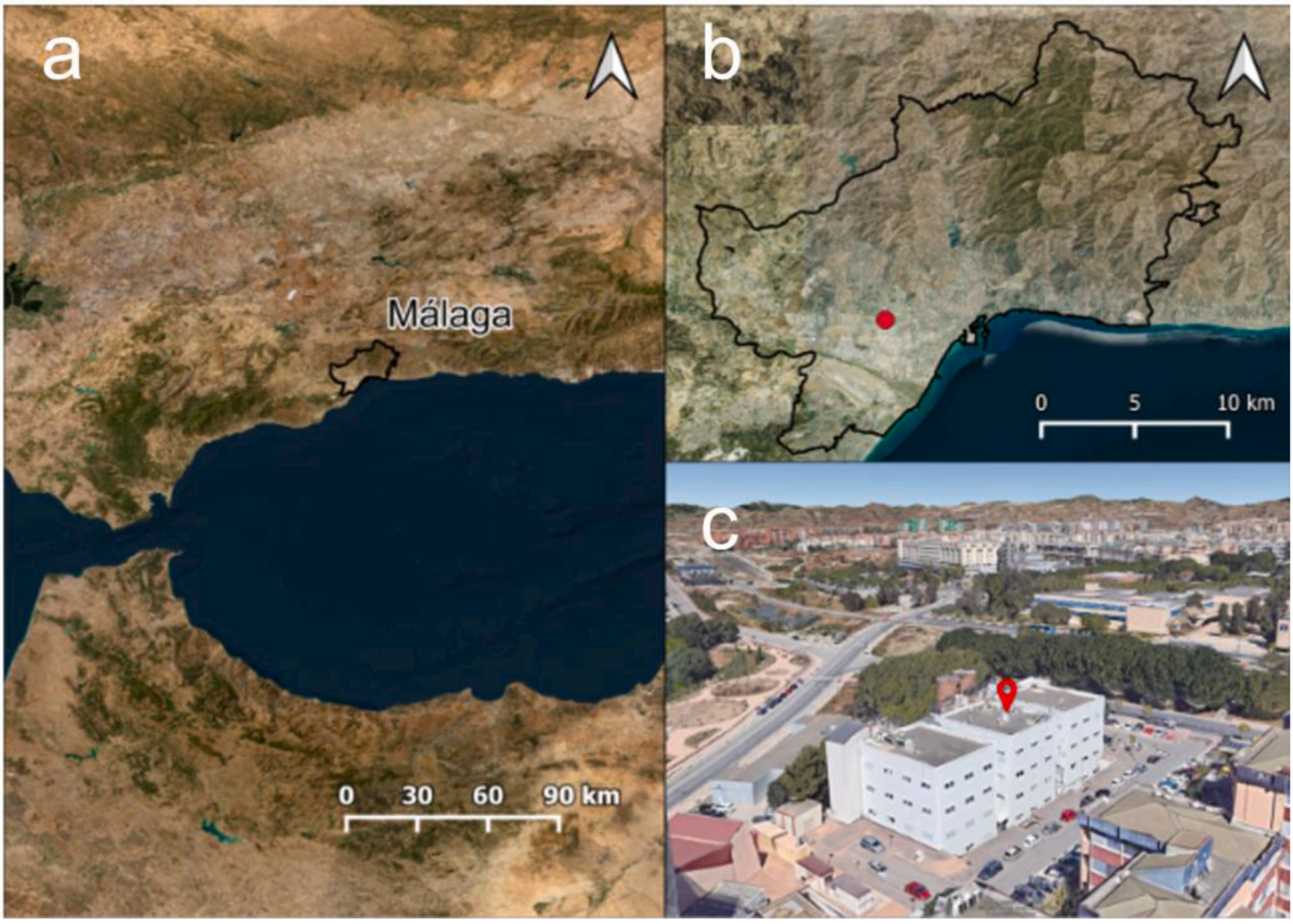

Fig. 1. (a) The coastal city of Málaga in southern Spain, on the Mediterranean shore (b) Location of sampling point (red point). (c) Two high-volume samplers are located on the roof of the Central Research Facilities Building (SCAI) at the University of Málaga. (For interpretation of the references to colour in this figure legend, the reader is referred to the Web version of this article.)

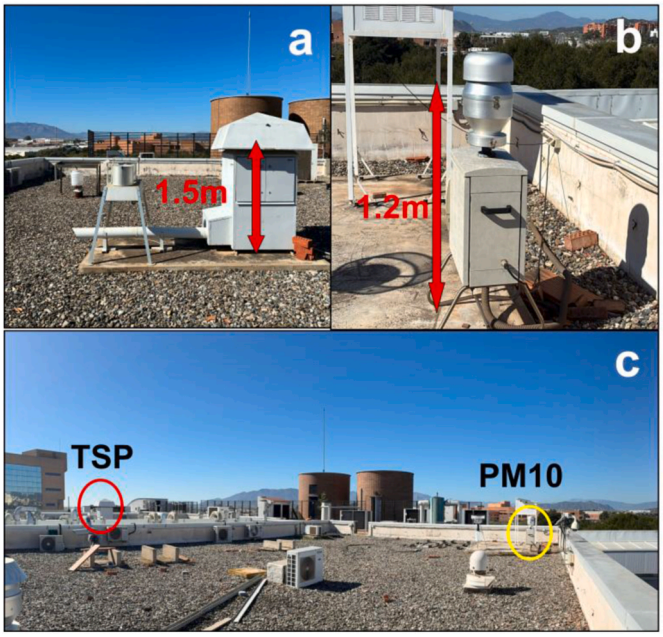

Fig. 2. High-volume samplers were used during study. a) and b) pictures depict PM_{10} and TSP samplers, respectively. Orange arrows show the distance of the filter holders from the roof floor; (c) panoramic image of the roof showing the distance between samplers. (For interpretation of the references to colour in this figure legend, the reader is referred to the Web version of this article.)

period, a total of 52 paired weekly samples (n = 52) of PM_{10} and TSP were collected and subsequently analysed under identical laboratory and counting conditions.

The samplers were installed on the roof of the Central Research Facilities Building (SCAI), at approximately 10 m above ground level. The rooftop consists of a flat gravel-ballasted roofing system, as illustrated in Fig. 2. Although gravel-covered roofs may allow limited accumulation of coarse dust, the sampling inlets were positioned well above the immediate surface layer, minimizing potential influence from local particle resuspension.

The PM_{10} and TSP samplers were installed approximately 10 m apart on an unobstructed rooftop platform. The inlets were positioned at heights of 1.2 m (PM_{10}) and 1.5 m (TSP) above the surface and oriented towards the predominant wind direction (see Fig. 2). After filtration, the air was exhausted downward through the base of each pumping unit. The separation distance, vertical inlet offset, and exhaust configuration minimize potential aerodynamic interference, shadowing effects, or recapture of filtered air between samplers. The vertical separation is small compared with the characteristic turbulent mixing scale above rooftop level and is not expected to generate systematic concentration gradients under typical atmospheric mixing conditions.

The PM_{10} fraction was collected using MCV/CAV-A/Mb high-volume sampler (MCV, S.A. https://mcvsa.com/en/products/) equipped with a PM_{10} size-selective inlet (50% aerodynamic cut-off at 10 μm), operating at a nominal flow rate of 30 m^3 h^{-1}. The inlet complies with the conventional PM_{10} sampling criteria based on aerodynamic diameter separation. Aerosols were retained on circular quartz microfiber filters (150 mm diameter, QMA type, MCV, S.A.), with a nominal particle retention efficiency higher than 99% for particles larger than 0.3 μm. In parallel, total suspended particles (TSP) were collected using a PTI high-volume sampler (model ASS-500), fitted with square polypropylene filters (440 mm side length type G-3, Physic-Technik-Innovation, PTI), designed for high-volume TSP aerosol collection.

The PM_{10} sampler operates at a fixed flow rate throughout the sampling period. In contrast, the TSP sampler does not include an automatic constant-flow controller. Due to progressive particle loading of the filter—particularly during Saharan dust intrusion events—the airflow typically decreased from approximately 700 m^3 h^{-1} at the start of sampling to about 350 m^3 h^{-1} at the end of the weekly collection period. To account for this variation, the total sampled air volume for each system was obtained directly from the calibrated volumetric flowmeter integrated into the sampler. Both flowmeters are periodically calibrated by the manufacturer following standard metrological procedures. Therefore, activity concentrations were calculated using the actual integrated air volume rather than nominal flow values, preventing systematic bias associated with flow rate reduction.

Although the filter retention efficiency exceeds 99% for the relevant particle size range, the overall sampling efficiency (including inlet aspiration and particle transmission) cannot be assumed to be strictly 100% under all atmospheric conditions. Differences in inlet design, flow regime, and particle-size-dependent aspiration efficiency may lead to slight variations in the effective collection of coarse particles. Since atmospheric ^{7}Be is predominantly associated with fine and submicron aerosols, both systems efficiently collect the fraction carrying most of the radionuclide activity. Consequently, minor deviations from the theoretical expectation TSP $\geq$ PM_{10} may occur without implying systematic bias or instrumental artefacts.

2.2. Gamma spectrometric analysis

After sampling, the filters were stored under controlled laboratory conditions for 96 h prior to gamma spectrometric analysis to allow for the complete decay of short-lived radon progeny (e.g., ^{214}Pb and ^{214}Bi) originating from ^{222}Rn. This waiting period prevents spectral interference and avoids potential overestimation of gamma-emitting radionuclides due to freshly deposited radon decay products. Given the half-life of ^{7}Be (53.3 days), this storage time does not introduce any significant decay bias.

Gamma-ray measurements were performed using a low-background coaxial high-purity germanium (HPGe) detector (GX3520; Canberra Industries Inc., USA) coupled to a Genie, 2000 spectral analysis system. The detector has a relative efficiency of 35% and an energy resolution of 0.83 keV at 122 keV and 1.75 keV at 1332 keV. The system was operated under recommended bias conditions and housed within a lead shielding assembly to minimize background radiation. ^{7}Be activity concentrations were determined via its characteristic gamma emission at 477.7 keV. Energy calibration was performed using certified reference sources, and full-energy peak efficiency calibration was conducted using a multi-gamma reference standard provided by the Research Centre for Energy, Environment and Technology (CIEMAT), Madrid, Spain. To exclude geometry-dependent artefacts, efficiency calibration was performed independently for each filter configuration (PM_{10} and TSP). The reference solution was homogeneously deposited onto clean filters of each type, reproducing the exact counting geometry of real samples. Independent efficiency calibration curves were thus obtained and applied to their corresponding sample sets.

Counting times ranged from 172,800 to 216,000 s, to ensure adequate counting statistics and minimize uncertainty. Minimum detectable activities (MDA) were calculated according to Currie (1968). Background subtraction and uncertainty propagation followed standard low-level gamma spectrometry procedures and according to the Spanish Nuclear Security Council's procedural document (Consejo de Seguridad Nuclear, 2025). Activity concentrations were corrected for radioactive decay to the midpoint of each sampling period and are reported in mBq m^{-3} with standard uncertainties (1σ), including contributions from counting statistics and efficiency calibration. This calibration and analytical approach ensure that observed differences in ^{7}Be concentrations between PM_{10} and TSP samples are not attributable to detector efficiency bias, counting geometry effects, or statistical treatment. Our laboratory regularly participates in inter-calibration tests in the field of gamma spectrometry organised by the International Atomic Energy Agency (IAEA), the Joint Research Centre (JRC), and the Spanish

National Security Council (CSN).

2.3. Meteorological data and statistical analysis

Meteorological data were obtained from a monitoring station operated by the Regional Government of Andalusia (Junta de Andalucía) in Campanillas (Málaga; 36°43′44″N, 4°33′38″W), located approximately 5 km west of the aerosol sampling site and considered representative of local atmospheric conditions. Datasets are publicly available on the Regional Government of Andalusia website. Daily meteorological data were processed to calculate mean air temperature (°C), cumulative precipitation (mm), mean wind speed (m s^{-1}), and mean wind direction over the same periods as the aerosol sampling. Since wind direction is a circular variable, it was transformed into its sine and cosine components prior to multivariate analysis to avoid discontinuity effects associated with angular measurements. Specifically, the cosine component was defined as Wind EW, representing the east–west directional component, and the sine component as Wind NS, representing the north–south directional component. These transformed variables were used in the statistical analysis instead of raw angular values.

These meteorological variables were analysed together with the measured ^{7}Be activity concentrations and aerosol mass concentrations to investigate their interrelationships and potential controlling factors. The statistical evaluation was performed using the complete dataset

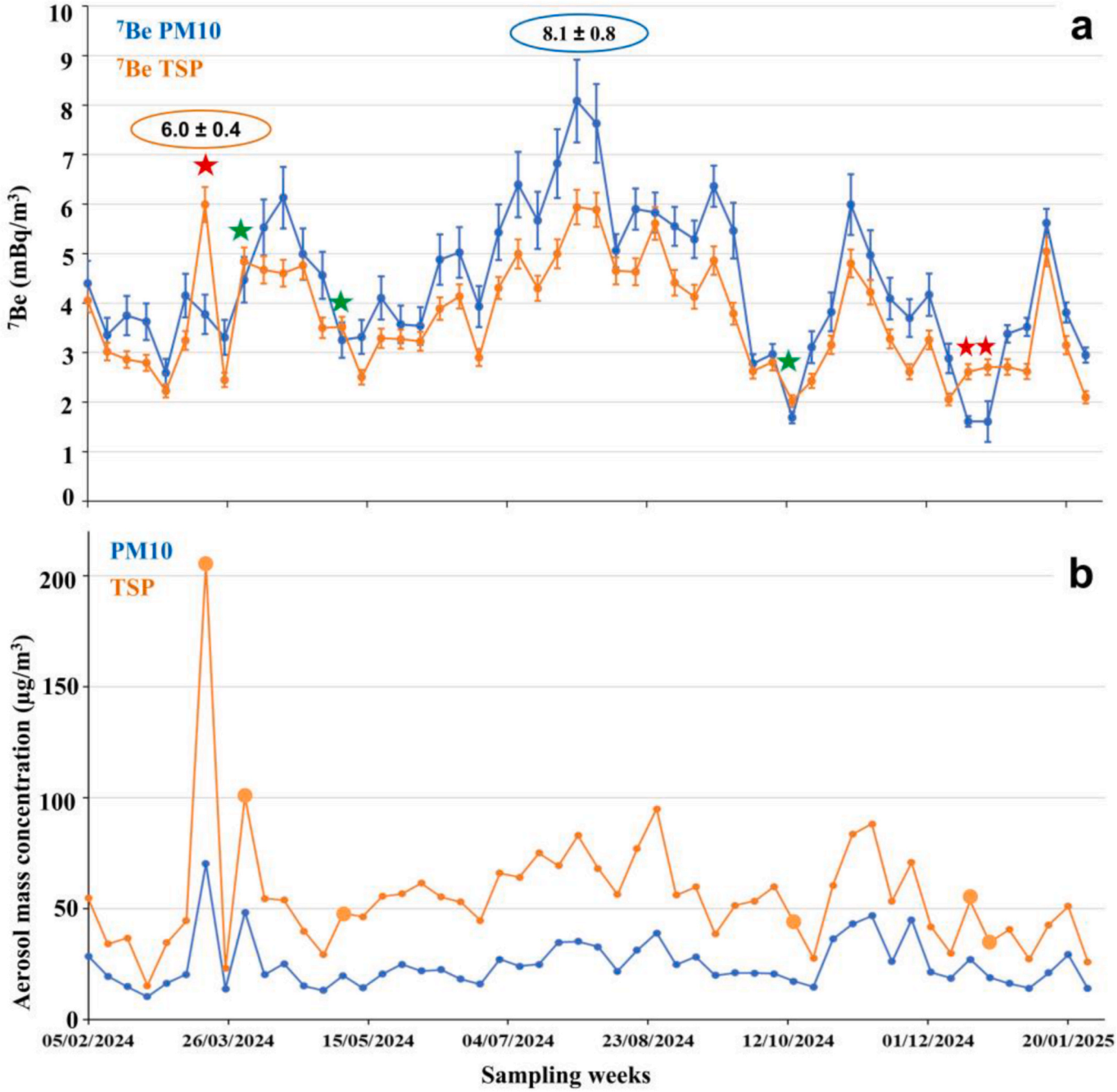

Fig. 3. (a) Temporal evolution of ^{7}Be activity concentrations (in mBq m^{-3}) measured in TSP and PM_{10} filters during the study period. Error bars represent standard uncertainties (1σ). Stars indicate sampling weeks in which ^{7}Be activity values in TSP exceed those of PM_{10} values (red stars indicate statistically significant differences). (b) Aerosol mass concentration (in µg m^{-3}) in TSP and PM_{10} filter samples. Bigger dots indicate sampling weeks in which ^{7}Be activity values exceed those of PM_{10} values. (For interpretation of the references to colour in this figure legend, the reader is referred to the Web version of this article.)

comprising 52 weekly observations (n = 52), corresponding to the paired PM_{10} and TSP samples collected during the study period. Correlation analysis was conducted using the Spearman rank correlation coefficient (ρ), given the non-normal distribution of several variables. In addition, multivariate statistical analysis was performed using factor analysis with VARIMAX rotation in SPSS (version 30.0). This method groups correlated variables into a reduced number of orthogonal components, thereby facilitating the identification of the dominant atmospheric processes influencing ^{7}Be behaviour and particulate matter dynamics during the study period.

2.4. Back-trajectory analysis

Air mass back-trajectory analyses were performed using the HYSPLIT (Hybrid Single-Particle Lagrangian Integrated Trajectory) model developed by the National Oceanic and Atmospheric Administration Air Resources Laboratory (ARL). Meteorological input data were obtained from the GDAS (Global Data Assimilation System) archive with 1° spatial resolution.

Four-day backward trajectories were computed for the Málaga sampling site for each day within selected weeks of interest. Trajectories were calculated at three arrival heights above ground level (AGL): 500 m, 1500 m, and 3000 m, to characterize transport pathways within the lower troposphere and assess the potential contribution of long-range transported air masses.

This multi-level approach enables discrimination between local/regional recirculation patterns and synoptic-scale advection, particularly during Saharan dust intrusion events. The analysis was specifically focused on sampling periods exhibiting statistically significant differences between TSP and PM_{10} ^{7}Be concentrations.

3. Results and discussion

3.1. Comparison between ^{7}Be activity concentrations in TSP and PM_{10}

Fig. 3 illustrates the weekly temporal evolution of ^{7}Be activity concentrations measured with the PM_{10} and TSP samplers throughout the study period. The similarity in the temporal behaviour of the two sampling systems is evident in the parallel fluctuations of the curves, and this agreement is quantitatively supported by a strong Spearman correlation ($\rho = 0.882$, $p < 0.001$). This high correlation demonstrates that both PM_{10} and TSP samplers respond consistently to changes in atmospheric conditions, validating their use for monitoring ^{7}Be in aerosol samples.

Both time series display comparable seasonal patterns and variability, with higher concentrations typically observed during spring and summer months and lower values in autumn and winter. This seasonal variability aligns with the known influence of atmospheric dynamics on the transport and deposition of cosmogenic radionuclides: enhanced vertical mixing and increased stratosphere–troposphere exchange during warmer periods generally lead to elevated surface ^{7}Be levels, whereas more stable conditions in cooler seasons result in reduced concentrations (e.g., Dueñas et al., 2015; Hernández Ceballos et al., 2016; Alegría Gutiérrez et al., 2020). The highest ^{7}Be activity concentration was observed during summer, including a peak of 8.1 ± 0.8 mBq m^{-3} in PM_{10} on 5-12 August 2024. Both ^{7}Be in PM10 and ^{7}Be in TSP exhibit moderate positive correlations with particle mass concentrations (PM_{10}: $\rho = 0.490$; TSP: $\rho = 0.637$; $p < 0.001$ in both cases). This relationship is expected, as higher aerosol loads provide greater surface area for radionuclide attachment and reflect atmospheric conditions conducive to particle accumulation. The stronger correlation observed for TSP may reflect the inclusion of coarser particles that contribute to overall mass variability.

Despite the strong temporal agreement between both datasets, ^{7}Be activity concentrations measured in PM_{10} samples tend to be higher than those obtained from TSP samples. For the entire study period, the mean activity concentrations were 3.7 ± 1.2 mBq m^{-3} for TSP and 4.4 ± 1.4 mBq m^{-3} for PM_{10}. A Wilcoxon signed-rank test indicated a statistically significant difference between the ^{7}Be activity concentrations measured in PM10 and TSP ($Z = -4.49$, $p < 0.001$), with higher activities observed in PM10 samples. Fig. 4 compares the distributions of ^{7}Be activity concentrations in TSP and PM_{10}. PM_{10} exhibits a higher median and a wider interquartile range, as well as a greater overall spread of values than TSP.

Although ^{7}Be activity concentrations measured in PM_{10} were generally higher than those obtained in TSP samples, six sampling periods showed TSP values exceeding PM_{10} (18–25 March, 1–8 April, 6–13 May, 14–21 October, 16–23 December, and 23–30 December). Statistical significance was evaluated by comparing the absolute difference between both measurements with their combined standard uncertainty. Differences were considered statistically significant when:

$$|A_{PM_{10}} - A_{TSP}| > \sqrt{u_1^2 + u_2^2} \quad [1]$$

where:

- A_{PM10} is the measured ^{7}Be activity concentration in the PM_{10} fraction (mBq m^{-3}),
- A_{TSP} is the measured ^{7}Be activity concentration in the TSP fraction (mBq m^{-3}),
- u_{PM10} is the standard uncertainty (1σ) associated with the PM_{10} measurement,
- u_{TSP} is the standard uncertainty (1σ) associated with the TSP measurement.

This criterion is based on the propagation of independent uncertainties and follows the principles established by Joint Committee for Guides in Metrology (JCGM/WG1), 2008 in the Guide to the Expression of Uncertainty in Measurement (GUM) (JCGM 100:2008), which provides the standard framework for combining uncertainties for addition and subtraction operations in metrological measurements. The term on the right-hand side of Eq. [1] represents the combined standard uncertainty of two independent measurements, obtained by quadratic summation. Only three sampling periods fulfilled this condition, exhibiting statistically significant higher ^{7}Be concentrations in TSP (18–25 March, 16–23 December, and 23–30 December). In the remaining cases, the observed differences were within the associated measurement uncertainties and therefore cannot be considered statistically significant.

Although individual weekly differences are not always statistically significant when measurement uncertainties are taken into account, the systematic shift observed in the distribution (Fig. 3) indicates a

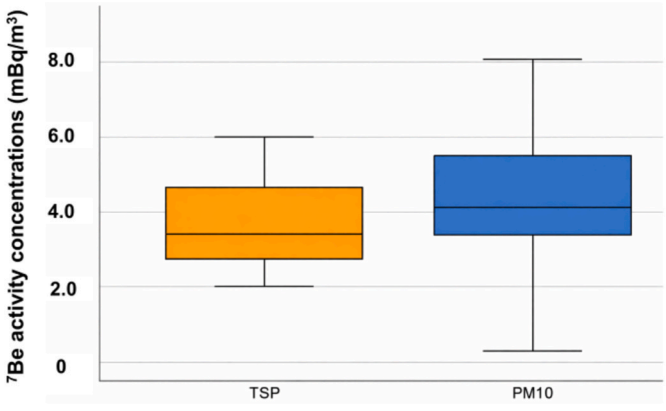

Fig. 4. Box-and-whisker plots of ^{7}Be activity concentrations in (TSP) and in the PM_{10} fraction (mBq m^{-3}). The central line within each box represents the median; the box limits correspond to the interquartile range (25th–75th percentiles), and the whiskers indicate the minimum and maximum values.

consistent tendency towards higher ^{7}Be values in the PM_{10} fraction. Relative differences between the two samplers range from 4% to 44%. This pattern suggests a preferential association of ^{7}Be with fine aerosol particles, consistent with the established production of cosmogenic radionuclides in the upper troposphere and lower stratosphere and their subsequent attachment to submicron particles (e.g., Papastefanou, 2009; Długosz-Lisiecka and Bem, 2020; Narazaki et al., 2021).

3.2. Meteorological influence and back-trajectory analysis

To characterize the prevailing atmospheric circulation during the study period, a wind rose analysis was performed. The results are presented in the Supplementary Material (Supplementary Fig. S1), showing a clear predominance of winds from the W–WNW sector, with secondary contributions from the NW sector. Less frequent but noticeable occurrences from the SE–SSE sector were also observed. The dominant westerly component reflects the regional synoptic circulation affecting the study area, whereas southeasterly episodes are consistent with episodic African air mass advection.

Correlation analysis was performed using the Spearman rank correlation coefficient to assess the relationship between ^{7}Be activity concentrations and meteorological variables. A significant positive correlation was observed between ^{7}Be activity and mean weekly air temperature for both particle fractions (PM_{10}: $\rho = 0.577$, $p < 0.001$; TSP: $\rho = 0.547$, $p < 0.001$). This indicates enhanced radionuclide concentrations under warmer atmospheric conditions, consistent with intensified vertical mixing and more efficient stratosphere–troposphere exchange processes. Precipitation showed significant negative correlations with ^{7}Be activity (PM_{10}: $\rho = -0.413$, $p = 0.002$; TSP: $\rho = -0.424$, $p = 0.002$), reflecting the scavenging effect associated with wet deposition, whereby rainfall removes aerosol-bound radionuclides from the atmosphere. Wind speed did not display a statistically significant correlation with ^{7}Be activity (PM_{10}: $\rho = -0.059$, $p = 0.680$; TSP: $\rho = -0.150$, $p = 0.287$), suggesting that local wind intensity alone is not a dominant driver of ^{7}Be variability. This behaviour is consistent with the cosmogenic origin of ^{7}Be and its preferential association with fine particles, whose variability is mainly controlled by large-scale atmospheric processes rather than mechanical resuspension. Wind direction was decomposed into its zonal (Wind EW) and meridional (Wind NS) components to avoid circular statistical artefacts. The zonal component (Wind EW) showed a significant negative correlation with ^{7}Be concentrations (PM_{10}: $\rho = -0.465$, $p < 0.001$; TSP: $\rho = -0.562$, $p < 0.001$), indicating that variations in the east–west circulation component significantly influence radionuclide variability. Considering the predominance of westerly winds in the study area, this suggests that specific synoptic circulation regimes modulate vertical mixing efficiency and long-range transport pathways. In contrast, the meridional component (Wind NS) did not show statistically significant correlations with ^{7}Be activity (PM_{10}: $\rho = -0.056$, $p = 0.693$; TSP: $\rho = -0.127$, $p = 0.369$), indicating that north–south airflow variability played a comparatively minor role during the study period.

A strong correlation was also observed between PM_{10} and TSP mass concentrations ($\rho = 0.890$, $p < 0.001$), confirming the coherence between both sampling inlets. Overall, the results indicate that ^{7}Be variability is primarily governed by temperature-related atmospheric mixing and large-scale zonal circulation patterns, while precipitation acts as an efficient removal mechanism and local wind speed has a limited direct influence.

Although ^{7}Be activity concentrations measured in PM_{10} were generally higher than those in TSP throughout the study period, six sampling weeks showed ^{7}Be activity values in TSP exceeding those in PM_{10} (18–25 March, 1–8 April, 6–13 May, 14–21 October, 16–23 December, and 23–30 December; see Fig. 3). Among these, three activity concentrations (18–25 March, 16–23 December, and 23–30 December 2024) exhibited statistically significant differences when considering combined standard uncertainties. Therefore, detailed trajectory analyses were focused on these three cases to clarify the atmospheric transport patterns associated with these sampling weeks (Fig. 5).

Back-trajectories for 18–25 March 2024 show a clear North African origin of the air masses at multiple arrival heights (500, 1500 and 3000 m), consistent with a well-defined Saharan dust intrusion. This week was characterised by the highest dust concentration observed in TSP filters during the study period (205 μg m^{-3}), together with the maximum ^{7}Be activity concentration in TSP (6.0 ± 0.4 mBq m^{-3}). The trajectory pattern and extreme aerosol loading jointly indicate that intense long-range transport of mineral dust substantially increased coarse particulate matter levels and modified aerosol size distribution, leading to a relative enhancement of ^{7}Be in the TSP fraction.

In contrast, the two December sampling weeks (16–23 and 23–30 December 2024) exhibit more complex transport patterns. Backward trajectories indicate predominantly continental and regional recirculation rather than a persistent North African pathway. Although these weeks did not present a clearly defined Saharan intrusion, regional resuspension processes and accumulation of locally or regionally derived coarse particles may enhance the relative contribution of the TSP fraction, thereby modifying radionuclide partitioning between PM_{10} and TSP without requiring long-range African transport.

The influence of mineral dust transport on radionuclide dynamics is further illustrated by the detection of ^{137}Cs in TSP filters during the March episode (18-25 March 2024), coinciding with the confirmed Saharan intrusion. During these days, a deep low-pressure system developed to the south-west of the Iberian Peninsula, affecting both surface and upper atmospheric levels. The associated circulation generated persistent southerly winds that favoured the transport of desert mineral dust across the Iberian Peninsula and the Balearic Islands. During this week, ^{137}Cs activity reached $(10 \pm 3)\bullet10^{-4}$ mBq m^{-3}, representing the maximum value recorded during the study year at the Málaga station and exceeding the minimum detectable activity. In the corresponding PM_{10} samples, the minimum detectable activity for ^{137}Cs under the applied counting conditions was $1.2\bullet10^{-2}$ mBq m^{-3}, approximately twice the activity measured in TSP. Therefore, although the absence of detectable ^{137}Cs in PM_{10} during this episode is in line with a preferential association of radiocaesium with the coarse aerosol fraction transported by mineral dust, the influence of lower sampled air volume and higher detection limits in the PM_{10} system cannot be entirely excluded.

Importantly, ^{137}Cs was detected in only three of the fifty-two analysed weeks, highlighting the episodic character of its atmospheric presence. The concurrence of enhanced coarse dust loading, detectable ^{137}Cs, and a statistically significant increase of ^{7}Be in TSP during the March intrusion supports the interpretation that Saharan dust outbreaks act as efficient mechanisms for the long-range transport of soil-derived radionuclides. Radiocaesium present in arid North African soils—originating from past atmospheric nuclear weapons testing and the Chernobyl accident—can be resuspended and transported over long distances during dust events, as documented in previous studies (Hernández et al., 2005, 2008; Liger et al., 2024).

Overall, these results demonstrate that while both PM_{10} and TSP sampling systems provide highly correlated measurements of ^{7}Be, particle size distribution becomes particularly relevant during episodes characterized by enhanced coarse particle transport. Synoptic conditions governing dust mobilization and air mass origin modulate radionuclide partitioning between size fractions, reinforcing the importance of combining trajectory analysis, radionuclide measurements, and aerosol mass data for a comprehensive interpretation of atmospheric transport processes.

3.3. Multivariate statistical analysis

To investigate the influence of meteorological conditions on ^{7}Be activity concentrations and dust levels, a factor analysis with VARIMAX rotation was performed. The results are presented graphically in Fig. 6,

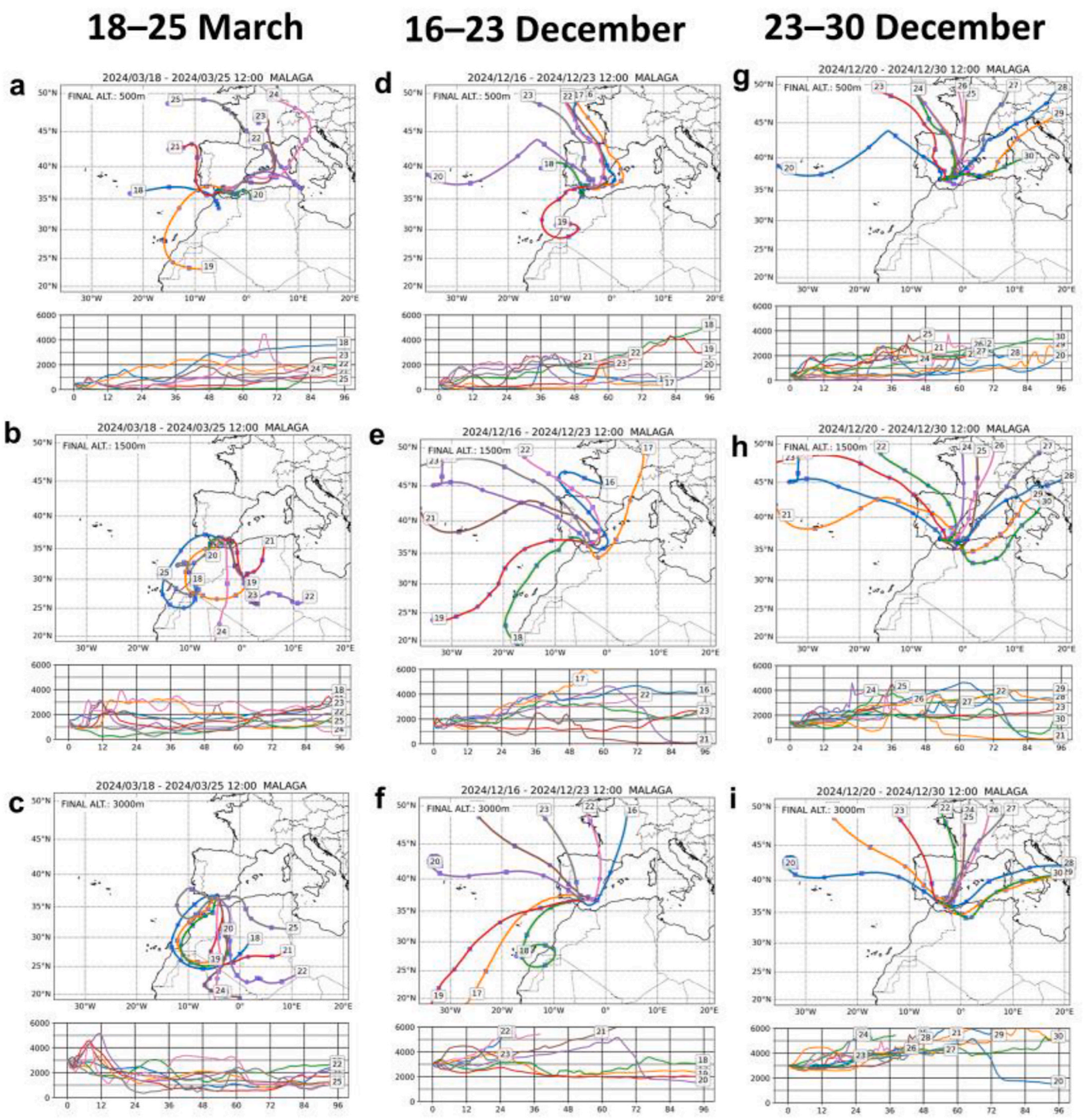

Fig. 5. Four-day HYSPLIT back-trajectories for 18-25 March (a-c), 16-23 December (d-f) and 23-30 December (g-i) 2024 arriving at Málaga sampling site at 12:00 UTC for three arrival heights (500, 1500 and 3000 m a.g.l.). The number in the rectangle corresponds to the day of arrival.

where the loadings of the analysed variables are projected onto the space defined by the first two principal components. These two components together explain approximately 70% of the total variance in the dataset.

The first component is characterized by high loadings of ^{7}Be activity concentrations in both PM_{10} (0.82) and TSP (0.88), together with temperature (0.83) and wind direction (EW) (−0.78), indicating that these variables jointly control the atmospheric behaviour and distribution of ^{7}Be at this site. The strong contribution of wind direction (EW) for component 1 agrees with the prevailing circulation pattern shown in the wind rose (Fig. S1), which reveals a dominant W–WNW flow with episodic southeastern contributions. This suggests that synoptic-scale air mass transport plays a central role in modulating surface ^{7}Be concentrations. Such behaviour is in accordance with the well-established origin of ^{7}Be in the upper troposphere and lower stratosphere, followed by downward transport through vertical air mass exchange and large-scale circulation processes. Similar associations between ^{7}Be, temperature, and synoptic-scale transport have been reported in previous studies, highlighting the role of atmospheric mixing and long-range transport in modulating surface-level ^{7}Be concentrations (e.g., Hernández et al., 2008; Papastefanou, 2009; Sýkora et al., 2016).

The second component shows strong associations between dust

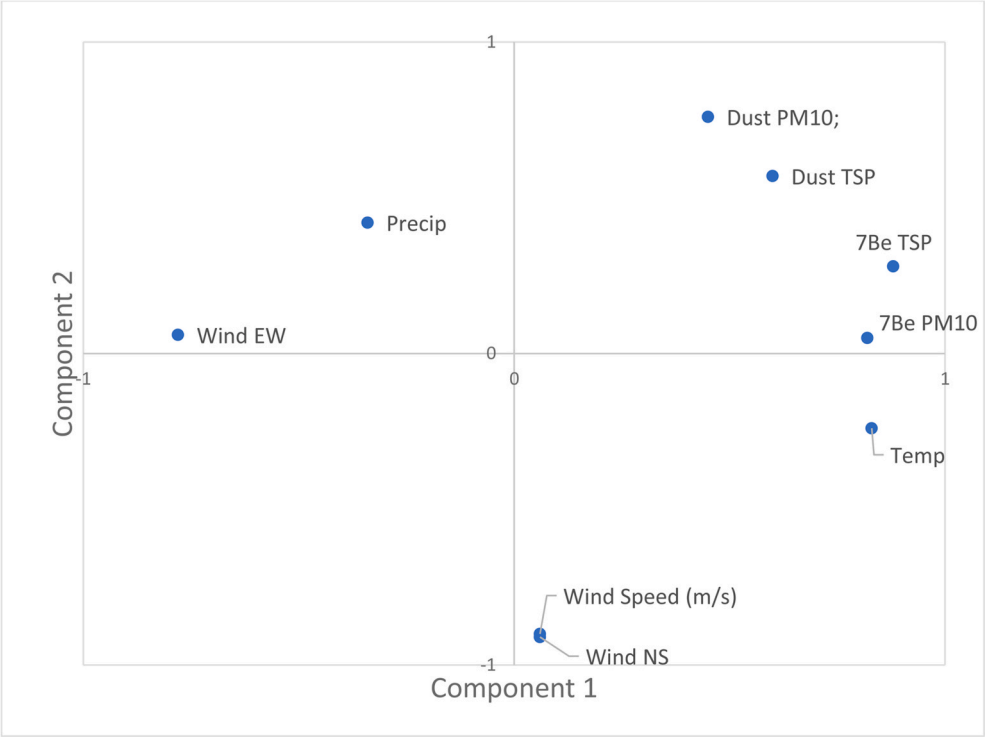

Fig. 6. Varimax-rotated factor-loading plot of the analysed variables projected onto the first two principal components. The diagram shows the relationship between ^{7}Be activity concentrations (PM_{10} and TSP), dust mass concentrations, and meteorological variables.

concentrations measured with the two samplers (0.76 in PM10; 0.76 in TSP) and wind speed (−0.90), highlighting the key role of wind in the transport, dispersion, and accumulation of particulate matter. This component reflects mechanical processes such as soil erosion, resuspension, and long-range advection, which are enhanced under high wind speed conditions, particularly during Saharan dust intrusion events. Similar factor structures linking dust loadings and wind speed have been documented in aerosol studies conducted in southern Spain and the Canary Islands, where African dust outbreaks are primarily driven by strong synoptic winds and regional circulation patterns (Querol et al., 2009).

The Varimax analysis reveals two distinct atmospheric control regimes. The first component represents a large-scale circulation and vertical mixing regime, characterised by strong contributions from ^{7}Be (both fractions), temperature, and the zonal wind component (Wind EW). This component is consistent with synoptic-scale modulation of cosmogenic radionuclide transport and downward mixing processes. The second component represents a mechanically driven aerosol regime, dominated by wind speed, the meridional wind component (Wind NS), and dust mass concentrations in both PM_{10} and TSP. This component captures the dynamic processes responsible for dust mobilisation, resuspension, and regional transport, particularly during Saharan intrusion events at the sampling site.

4. Conclusions

This study provides a comparison of ^{7}Be activity concentrations measured using PM_{10} and TSP aerosol sampling systems under urban background conditions. By explicitly accounting for methodological factors associated with aerosol collection efficiency, detector performance, and sampling temporal resolution, the adopted analytical approach reduces interpretative bias associated with procedural variability and strengthens the robustness of the comparison.

Mean ^{7}Be concentrations during the study were 4.4 ± 1.4 mBq m^{-3} for PM_{10} and 3.7 ± 1.2 mBq m^{-3} for TSP, with a strong temporal correlation between both datasets ($\rho = 0.882$, $p < 0.001$). Although weekly differences were generally not statistically significant when considering combined standard uncertainties (1σ), a persistent tendency toward higher ^{7}Be values in the PM_{10} fraction was clearly observed. This systematic difference, reaching up to 44% in relative terms, indicates that inlet-dependent size selectivity can influence reported concentrations even under comparable environmental conditions. Previous studies have shown that ^{7}Be is predominantly associated with fine and accumulation-mode aerosols, which explains the generally higher activities measured in PM_{10} samples under typical atmospheric conditions. (Papastefanou, 2009; Baskaran, 2011).

Only three weekly sampling periods exhibited statistically significant higher ^{7}Be concentrations in TSP. Back-trajectory analysis showed that a clear North African intrusion was evident in only one of these episodes (March), whereas the two December cases were not associated with well-defined Saharan transport patterns. This suggests that while intense dust intrusions can enhance coarse-mode radionuclide transport, additional meteorological mechanisms may also contribute to temporary shifts in aerosol size partitioning.

The detection of ^{137}Cs in TSP during the March intrusion, reaching (10 ± 3) •10^{-4} mBq m^{-3} (the highest value recorded during the study year), further supports the role of long-range dust transport in mobilising soil-derived radionuclides. During the same week, ^{137}Cs remained below the minimum detectable activity in PM_{10} samples (1.2•10^{-2} mBq m^{-3}). Although this behaviour is in line with preferential association of radiocaesium with the coarse aerosol fraction transported during dust outbreaks, the influence of sampling volume and detection limits in the PM_{10} system cannot be entirely excluded.

Multivariate analysis using VARIMAX rotation identified two principal components explaining approximately 70% of the total variance. The first component linked ^{7}Be concentrations primarily with temperature and atmospheric transport patterns, reflecting the influence of large-scale circulation and vertical exchange processes. The second component associated dust levels with wind speed, highlighting the importance of mechanical transport and resuspension dynamics.

Independent analyses performed separately for PM_{10} and TSP confirmed the stability of the factor structure.

Overall, both PM_{10} and TSP sampling systems provide robust and highly correlated measurements of atmospheric ^{7}Be activity concentrations, indicating that either configuration can reliably capture the general variability of this cosmogenic radionuclide. However, differences in particle size distribution, particularly during episodic dust intrusions, may alter radionuclide partitioning across aerosol fractions and thus introduce systematic discrepancies when datasets obtained using different inlet configurations are directly compared. These results highlight the importance of considering aerosol size fraction and sampling inlet characteristics when integrating or inter-comparing atmospheric radionuclide datasets obtained using different sampling configurations.

CRediT authorship contribution statement

E. Gordo: Writing – original draft, Methodology, Investigation, Formal analysis. **E. Liger:** Writing – review & editing, Supervision. **E.M. Navarro:** Writing – review & editing. **J. Rodríguez-Jiménez:** Writing – review & editing.

Declaration of competing interest

The authors declare the following financial interests/personal relationships which may be considered as potential competing interests: ELISA GORDO PUERTAS reports financial support was provided by Nuclear Safety Council. If there are other authors, they declare that they have no known competing financial interests or personal relationships that could have appeared to influence the work reported in this paper.

Acknowledgments

This work has been partially supported by the Spanish Nuclear Safety Council (CSN). The authors gratefully acknowledge the NOAA Air Resources Laboratory (ARL) for the provision of the HYSPLIT transport and dispersion model and/or READY website (https://www.ready.noaa.gov) used in this study. The authors thank Dr. Francisco J. Expósito from the University of La Laguna (GOTA research group) for assistance with the back-trajectory analyses and their interpretation.

Appendix A. Supplementary data

Supplementary data to this article can be found online at https://doi.org/10.1016/j.jenvrad.2026.107962.

Data availability

Data will be made available on request.

References

Alegría Gutiérrez, N., Hernández-Ceballos, M.Á., Herranz, M., Idoeta, R., Legarda, F., 2020. Meteorological factors controlling ^{7}Be acbivity concentrations in the atmospheric surface layer in northern Spain. Atmosphere 11, 1340. https://doi.org/10.3390/atmos11121340.

Baskaran, M., 2011. Po-210 and Pb-210 as atmospheric tracers and global atmospheric Pb-210 fallout: a review. J. Environ. Radioact. 102, 500–513. https://doi.org/10.1016/j.jenvrad.2010.10.007.

Błażej, S., Mietelski, J.W., 2014. Cosmogenic 22Na, ^{7}Be anb terrestrial 137Cs, 40K radionuclides in ground level air samples collected weekly in Kraków (Poland) over years 2003–2006. J. Radioanal. Nucl. Chem. 300, 747–756. https://doi.org/10.1007/s10967-014-3049-6.

Consejo de Seguridad Nuclear, 2005. Procedimiento de muestreo y preparación de muestras para la determinación de la radiactividad en aerosoles y radioyodos. Procedimiento 1.7.

Consejo de Seguridad Nuclear, 2025. Procedimiento de muestreo y preparación de muestras para la determinación de la radiactividad en aerosoles y radioyodos. Procedimiento 1.7. Rev. 1, 2025) [Environmental radiological monitoring. Procedure 1.7 (Rev. 1, 2025)]. In: https://www.csn.es/documents/10182/27786/INT-04-07+Vigilancia+radiol%C3%B3gica+ambiental+Procedimiento+1.7.+%28Rev.+1%2C+2025%29/435c4c4c-8eac-48b4-bf9c-2df897539832.

Currie, L.A., 1968. Limits for Qualitative Detection and Quantitative Determination, Application to Radiochemistry. Anal. Chem. 40, 586–593. https://doi.org/10.1021/ac60259a007.

Dibb, J., Talbot, R.W., Scheuer, E., Seid, G., DeBell, L., Lefer, B., Ridley, B., 2003. Stratospheric influence on the northern North American free troposphere during TOPSE: ^{7}Be asba stratospheric tracer. J. Geophys. Res. Atmos. 108. https://doi.org/10.1029/2001JD001347.

Długosz-Lisiecka, M., Bem, H., 2020. Seasonal fluctuation of activity size distribution of 7Be, 210Pb and 210Po radionuclides in urban aerosols. J. Aerosol Sci. 144, 105544. https://doi.org/10.1016/j.jaerosci.2020.105544.

Dueñas, C., Orza, J.A.G., Cabello, M., Fernández, M.C., Cañete, S., Pérez, M., Gordo, E., 2011. Air mass origin and its influence on radionuclide activities (7Be and 210Pb) in aerosol particles at a coastal site in the western Mediterranean. Atmos. Res. 101, 205–214. https://doi.org/10.1016/j.atmosres.2011.02.011.

Dueñas, C., Fernández, M.C., Cabello, M., Cañete, S., Pérez, M., Gordo, E., 2015. Study of the cosmogenic factors influence on temporal variation of 7Be air concentration during the 23rd solar cycle in Málaga (South Spain). J. Radioanal. Nucl. Chem. 303, 2151–2158. https://doi.org/10.1007/s10967-014-3737-2.

Feely, H.W., Larsen, R.J., Sanderson, C.G., 1989. Factors that cause seasonal variations in beryllium-7 concentrations in surface air. J. Environ. Radioact. 9, 223–249. https://doi.org/10.1016/0265-931X(89)90046-5.

Genie, 2000. Spectroscopy System Operations. Canberra Industries.

Gordo, E., Dueñas, C., Fernández, M.C., Liger, E., Cañete, S., 2015. Behaviour of ambient concentrations of natural radionuclides 7Be, 210Pb and 40K in the Mediterranean coastal city of Málaga (Spain). Environ. Sci. Pollut. Res. 22, 7653–7664. https://doi.org/10.1007/s11356-014-4039-5.

Hernández, F., Alonso-Pérez, S., Hernandez-Armas, J., Cuevas, E., Karlsson, L., Romero-Campos, P.M., 2005. Influence of major African dust intrusions on the 137Cs and 40K activities in the lower atmosphere at the Island of Tenerife. Atmos. Environ. 39, 4111–4118. https://doi.org/10.1016/j.atmosenv.2005.03.032.

Hernández, F., Rodríguez, S., Karlsson, L., Alonso-Pérez, S., López-Pérez, M., Hernández-Armas, J., Cuevas, E., 2008. Origin of observed high 7Be and mineral dust concentrations in ambient air on the Island of Tenerife. Atmos. Environ. 42, 4247–4256. https://doi.org/10.1016/j.atmosenv.2008.01.017.

Hernández-Ceballos, M.A., Brattich, E., Cinelli, G., Ajtić, J., Djurdjevic, V., 2016. Seasonality of 7Be concentrations in Europe and influence of tropopause height. Tellus B Chem. Phys. Meteorol. 68, 29534. https://doi.org/10.3402/tellusb.v68.29534.

Ioannidou, A., Paatero, J., 2014. Activity size distribution and residence time of 7Be aerosols in the Arctic atmosphere. Atmos. Environ. 88, 99–106. https://doi.org/10.1016/j.atmosenv.2013.12.046.

Ioannidou, A., Papastefanou, C., 2020. Beryllium-7 concentrations in the lower atmosphere in the region of Thessaloniki (40°N). HNPS Adv. Nucl. Phys. 5, 185–195. https://doi.org/10.12681/hnps.2902.

Joint Committee for Guides in Metrology (JCGM/WG1), 2008. Evaluation of measurement data: guide to the expression of uncertainty in measurement (GUM). JCGM 100, 2008, BIPM.

Koch, D., Jacob, D.J., Graustein, W.C., 1996. Vertical transport of tropospheric aerosols as indicated by 7Be and 210Pb in a chemical tracer model. J. Geophys. Res. Atmos. 101, 18651–18666. https://doi.org/10.1029/96JD01176.

Lal, D., Peters, B., 1967. Cosmic ray produced radioactivity on the Earth. In: Sitte, K. (Ed.), Handbuch Der Physik, 46/2. Springer, Berlin, pp. 551–612. https://doi.org/10.1007/978-3-642-46079-1_7.

Liger, E., Hernández, F., Expósito, F.J., Díaz, J.P., Salazar-Carballo, P.A., Gordo, E., González, C., López-Pérez, M., 2024. Transport and deposition of radionuclides from northern Africa to the southern Iberian Peninsula and the Canary Islands during the intense dust intrusions of March 2022. Chemosphere 352, 141303. https://doi.org/10.1016/j.chemosphere.2024.141303.

Narazaki, Y., Sakoda, A., Takahashi, S., Momoshima, N., 2021. Cosmogenic 7Be: particle size distribution and chemical composition of 7Be-carrying aerosols in the atmosphere in Japan. J. Environ. Radioact. 237, 106690. https://doi.org/10.1016/j.jenvrad.2021.106690.

Papastefanou, C., 2006. Residence time of tropospheric aerosols in association with radioactive nuclides. Appl. Radiat. Isot. 64, 93–100. https://doi.org/10.1016/j.apradiso.2005.07.006.

Papastefanou, C., 2009. Beryllium-7 aerosols in ambient air. Aerosol Air Qual. Res. 9, 187–197. https://doi.org/10.4209/aaqr.2009.01.0004.

Querol, X., Pey, J., Pandolfi, M., Alastuey, A., Cusack, M., Pérez, N., Moreno, T., Viana, M., Mihalopoulos, N., Kallos, G., Kleanthous, S., 2009. African dust contributions to mean ambient PM10 mass levels across the Mediterranean Basin. Atmos. Environ. 43, 4266–4277. https://doi.org/10.1016/j.atmosenv.2009.06.013.

Sýkora, I., Holý, K., Ješkovský, M., Müllerová, M., Bulko, M., Povinec, P., 2016. Long-term variations of radionuclides in Bratislava air. J. Environ. Radioact. 166, 27–35. https://doi.org/10.1016/j.jenvrad.2016.03.004.

UNSCEAR, 2000. Sources and Effects of Ionizing Radiation. United Nations Scientific Committee on the Effects of Atomic Radiation. United Nations, New York.